Electrical characterization of defects induced by electron beam exposure in low doped *n*-GaAs

S.M. Tunhuma, F.D. Auret, J.M. Nel, E. Omotoso, H.T. Danga, E. Igumbor and M. Diale

Department of Physics, University of Pretoria, Private Bag X20, Pretoria 0002, South Africa

Corresponding author: S. M. Tunhuma malven.tunhuma@up.ac.za +27844314906

Abstract

We have used deep level transient spectroscopy (DLTS) and Laplace DLTS (L-DLTS) to characterize the electrically active point defects introduced in *n*-type gallium arsenide by electron beam exposure prior to Schottky metallization. The GaAs crystals were exposed to incident electrons at sub-threshold energies which are deemed low and insufficient to form defects through ion solid interactions. DLTS revealed a set of electron traps different from those commonly observed in *n*-GaAs after particle irradiation. These different signatures from the same radiation type suggest that different mechanisms are responsible for defect formation in the two electron irradiation processes. An analysis of the conditions under which the defects were formed was done to distil a number of possible defect formation mechanisms using the experimental evidence obtained.

Introduction

Defect formation in semiconductors at sub-threshold energies has been a subject of interest for a considerable period of time [1]. Threshold energy is the minimum amount of energy a lattice atom will receive before being displaced to a stable interstitial position at low temperatures and has been shown to be approximately 9.0 eV in Ga and 9.4 eV in As [2].

Previous studies have focused on explaining the formation of defects in the electron beam physical vapour deposition (EB-PVD) metallization process on semiconductors at low incident energies [3-6]. Ning, [3] speculated that X-rays originating when electrons strike a metal target interact with the semiconductor material resulting in defect formation. Nel and Auret [4] attributed the damage to stray electrons in the deposition chamber and postulated that another process other than elastic scattering was responsible for the formation of the defect species, since momentum conservation could not account for sub-lattice collisions and a cascade of displacements [7]. Christensen *et.al* [5] speculated that low energy ions produced close to the filament when electrons collide with residual gas atoms interact with the sample and introduce defects. Recently Archila *et.al* [8] speculated that intrinsic non-localized excitations modify defects deeper in the surface rendering them observable and

concluded that energy can travel in a germanium lattice through wave packets and deliver energy to produce defects.

Studies in silicon, germanium and 4*H* silicon carbide have demonstrated that electron beam exposure (EBE) induces defects in the particular semiconductors but with different conclusions [6, 9, 10]. There is therefore still a need to carry out some more investigations and establish concrete evidence on the fundamental physics of defect formation. Gallium arsenide is polar and radiation hard hence it presents a good platform to substantiate most recent experimental observations and theories. Quantitative insights on the nature and occurrence of these defects, wave functions of localised carriers, energy spectra and elementary excitations is vital for semiconductor crystal growth and utilization.

In this work we have investigated the mechanisms responsible for defect formation in MOVPE grown *n*-GaAs by comparing defect signatures. By adopting and modifying the physical vapour deposition process, GaAs samples were exposed to sub-threshold energy electrons from an electron gun. The resulting defects were compared to those induced by high energy electron irradiation (HEEI) and electron beam physical vapour deposition (EB -PVD).

Experimental procedure

The samples studied were silicon doped *n*-GaAs <100> with an average carrier density of 1.0×10^{15} cm^{-3} (MOVPE) grown, on n^+ substrates, supplied by Spire Corporation. Wafers were degreased and etched chemically. A Au-Ge (88 %:12 %) eutectic was resistively deposited on the n^+ sides and annealed for 2 minutes in Ar at 450 ℃ to form an ohmic contact.

Thereafter the samples were cut into 1 cm^2 pieces and some were exposed to an electron beam with a current of approximately 100 mA from a A 10 keV (MDC model e-Vap 10CVS) electron gun for 1 hour. This was achieved in an EB-VPD system by creating conditions similar to those for physical vapour deposition. A schematic diagram of the setup is illustrated in Fig. 1. In the diagram the arrow shows the path traced by the electron beam towards the metal target. The electron beam was heating the tungsten at energy levels insufficient to evaporate the metal, a technique termed electron beam exposure (EBE) [9]. Shielding was adopted to avoid exposure of the sample to any energetic particles in the electron beam path or stray electrons.

The chamber pressure was approximately 1×10^{-4} mbar. Thereafter 1000 Å thick Au circular contacts, 0.6 mm in diameter, were deposited on the epitaxial layer using resistive evaporation to form Schottky barrier diodes (SBDs). Au was used to ensure that the defects were process induced and not material related. Comparison and control of the results was done using the following samples:

1. 1000 Å circular Au contacts, 0.6 mm in diameter were deposited on the epitaxial layer using resistive evaporation (RE) in an Edwards AUTO 306 system pumped down at 2.5×10^{-6} mbar. These samples were used as references because resistive evaporation (RE) of Au does not introduce any detectable electrically active defects in GaAs and it therefore gives a very accurate result on the defect content of the as-deposited sample. It also easily compares to the Au that was deposited on EBE samples after exposure.
2. Samples were irradiated with MeV electrons for 1 hour up to a fluence of 2.48×10^{13} cm^{-2} and Au Schottky contacts were fabricated on the epitaxial layer using RE. A detailed graphical representation of electron energies emitted by the radionuclide is given by Auret *et.al* [9].
3. Tungsten Schottky contacts 0.6 mm in diameter were fabricated using EB-PVD in the chamber illustrated in Fig. 1. The same electron gun used for EBE with a higher beam current of ~250 mA was used to deposit a total thickness of 1000 Å. Tungsten was used because it was the target metal for the EBE.

Contact quality was evaluated using current-voltage *(I-V)* and capacitance-voltage *(C-V)* measurements. Assuming pure thermionic emission, and for $V > 3kT/q$ the relationship between the current I and the applied bias voltage V is given by [11]:

$$I = AA^{*}T^{2} \exp\left(\frac{q\phi_0}{kT}\right)\left[\exp\left(\frac{q(V - IR_S)}{nkT}\right) - 1\right] \tag{1}$$

where q is the electronic charge, k the Boltzmann constant, T the absolute temperature, R_s the series resistance, $\phi_0 (=\phi_{IV})$ the zero-bias barrier height obtained from

$$\phi_0 = \frac{kT}{q} \ln \frac{AA^{*}T^{2}}{I_s} \tag{2}$$

A the diode area, *n* the ideality factor and A^*(=8.16 $Acm^{-2}K^{-2}$) the Richardson`s constant. The *C-V* analysis was done using the Schottky Mott theory [11]

$$C^{-2} = \frac{2(V_{bi} - V)}{q\varepsilon_s A^2 N_D} \tag{3}$$

where N_D is the free carrier concentration and ε_s is the permittivity of the semiconductor. The *C-V* barrier height is given by $\phi_{CV} = v_{bi} + v_0$ where v_{bi} is the diffusion potential extracted from a C^{-2}-*V* plot and v_0 is the potential difference between the conduction band minima and the conduction band of the Fermi level in the neutral part of the semiconductor.

DLTS spectra were recorded at a scan rate of 2 K/min in the 15 – 320 K temperature range. The quiescent reverse bias was –1 V, filling pulse amplitude between 0 < *V* < -0.2 V below the 0 V reference and filling pulse width 1 ms. The fine structure of the defects was then investigated using Laplace-DLTS . The signatures (energy level in the band gap, E_T and apparent capture cross section, σ_n) of the induced defects were calculated from the slope and *y*-intercept, respectively using log (e_n/T^2) versus (1000/*T*) Arrhenius` plots, according to the equation [12]

$$e_n = \sigma_n \langle v_n \rangle \frac{g_o}{g_1} N_c \exp\left(-\frac{E_C - E_T}{k_B T}\right) \tag{4}$$

This equation gives the emission rate as a function of temperature *T*, where $\langle v_n \rangle$ is the thermal velocity of electrons, (E_C – E_T) is the activation energy. N_c is the density of conduction band states, g_0 and g_1 are the degeneracy terms referring to the states before and after electron emission and k_B is the Boltzmann constant.

In the technique, each defect has a unique identifier which is the capture cross section and the activation energy. When different processes are involved in inducing or forming the same defect the electronic properties act as a “signature” which can be used for identification.

Results and discussion

Current-voltage and capacitance-voltage results.

Fig. 2. shows the *I-V* characteristics of the devices measured in this investigation. The results from both the *I-V* characteristics and the *C-V* characteristics are summarised in Table 1 together with the name of the contact metal. It is worth noting that the difference in work

function between tungsten and gold will also contribute to a relatively lower barrier in tungsten based devices. Besides this no chemical reactions were expected between GaAs and these metals. Ideally good quality Schottky contacts on low doped gallium arsenide should have forward bias *I-V* characteristics that closely follow the thermionic emission model [13]. An ideality factor (*n*) close to 1 was therefore expected. For all processes listed in Table 1 ϕ_{CV} was observed to be higher than ϕ_{IV}. This was attributed by Werner and Guttler to spatial variations in the barrier which cause current to preferentially flow through band minima resulting in a lower measured ϕ_{IV} [14]. The EBE and EB-PVD samples have the highest reverse leakage current which shows poor rectification properties compared to the other samples.

The control devices made by resistive evaporation had good characteristics with an ideality factor of almost unity. EBE processed devices exhibited diode characteristics that were closest to those of SBDs fabricated with resistive evaporation. This shows that there was a moderate to low effect on the diode characteristics by the EBE. Among other changes, incident particles have been known to introduce change in surface stoichiometry which can introduce surface states and change the position where the Fermi level is pinned [15]. These surface states can contribute to barrier alteration.

Devices made by the EB-PVD of tungsten had a higher reverse leakage than the rest of the devices. Flattening of the *I-V* curve above 0.5 V in Fig. 2. shows that the devices had a higher series resistance. In addition, the EB-PVD data recorded in Table 2 also shows relatively lower barrier heights (ϕ_{IV} and ϕ_{CV}) relative to RE which might be a result of both radiation effects and the lower work function of tungsten when compared to gold. These results confirm that EB-PVD degrades diode characteristics. A higher value of *n* suggests the presence of other current transport mechanisms such as generation-recombination. Comparison with the EBE results shows that the damage introduced by tungsten particles cannot be overlooked in the EB-PVD process. The technique has been shown to introduce near surface defect states that result in non-ideal diode characteristics [16].

The plot from HEEI devices also shows degradation of electrical characteristics. Although the high energy particles influenced the electrical characteristics of the diodes, this was not as significant as that of EB-PVD. The difference in the level of degradation to EBE, and EB-PVD can be attributed to the depth of the damage into the junction. In total, the EBE and EB-PVD had a significant impact on *I-V* and *C-V* characteristics of SBDs. A similar result was

observed by Omotoso *et.al* in 4*H*-SiC [17, 18]. However the quality was good enough for DLTS analysis.

DLTS results

The defects introduced by the various processes were characterised using DLTS. Fig. 3. shows the DLTS spectra of SBDs measured in the 20-320 K temperature range. The signatures were determined from the Arrhenius plots in Fig. 4. The attributes of all the traps are listed in Table 2. The reference spectrum (a) obtained from RE samples indicates there were no detectable defects in the samples within the measured range. Curve (b) shows the EB-PVD induced defects in GaAs. These are the $E_{0.43}$ and a broad base peak around 200 K which was observed by Auret *et.al* in Pd/n-GaAs Schottky diodes fabricated by EB-PVD and they speculated that it was a continuum of defect states [19].

The EBE and HEEI induced defects are shown in spectra (c) and (d) respectively. A comparison of the two spectra and the defect properties in Table 2 shows that the defects are different even though they are in both cases induced by electrons. Whilst a similar contrast has been also observed in germanium and silicon a different result was observed in 4*H*-SiC where both EBE and HEEI defects had the same signatures [10]. None of the defects commonly observed after particle irradiation in the past have identical electronic properties to the EBE defects. The EB-PVD and EBE spectra in Fig. 3., although carrying the same number of peaks, have a clear temperature shift between them when compared to each other showing that the EBE induced defects are unique and carry different signatures. At this point we can therefore conclude that different mechanisms are responsible for the formation of these defects.

We also speculate that the broad based peak on spectrum (c) observed around 240 K is a continuum of defect states close to the junction because its Laplace-DLTS spectra show a number of peaks which vary inconsistently with temperature. According to Naber, [20] this continuum of defect states can either be a result of surface effects, displacement of lighter impurities which displace host atoms or displacements near dislocations or other structural defects [20]. Whilst surface patterning has been observed in gallium arsenide by Bischoff *et al* [21] and can give rise to a similar detection of defect states, the sizes of the electrons used in this experiment were too small compared to the sizes of high energy particles used in their experiments. We cannot thus conclude that surface patterning gave rise to the continuum of defect states.

The path of the electron beam was closed by shielding in the EBE experiment. This allows us to rule out the possibility of the defects being formed by X-rays or by stray electrons from the electron gun. However the viewpoint of Christensen *et.al* that ions formed close to the filament may be responsible for defect formation when they interact with the sample remains a potential cause of the formation of these defects. The energies involved were very low for Frenkel pair formation therefore other theories like the vibrational nodes speculated by Archila *et.al* could explain the energy transfer. The quality of the surface and cleanliness also contributes to the surface damage threshold [22].

Conclusions

Current-voltage and capacitance-voltage measurements showed that electron beam exposure degrades the quality of Schottky diodes fabricated on GaAs. Laplace-Deep level transient spectroscopy revealed that electron beam exposure (EBE) results in the formation of the $E_{0.34}$ defect and a continuum of defect states observed around 240 K whilst high energy electron irradiation (HEEI) induces the $E_{0.14}$, $E_{0.17}$, $E_{0.38}$ and $E_{0.63}$. The EBE defects were different to those observed after HEEI or electron beam deposition. They were also different to any other defects observed in previous studies on GaAs suggesting that they are formed by a unique mechanism. X-rays and stray electrons were ruled out as the causatives of the defect formation. We therefore conclude that EBE at sub-threshold energies results in the formation of defects in *n*-GaAs and must be avoided in the industrial fabrication of devices.

Acknowledgements

The authors would like to thank the South African National Research Foundation (NRF) and the University of Pretoria for financial support.

References

[1] V. Vavilov, A. Kiv, O. Niyazova, The subthreshold radiation effects in semiconductors, Physica status solidi (a), 32 (1975) 11-33.
[2] J.H. Crawford, L.M. Slifkin, Point Defects in Solids: Volume 2 Semiconductors and Molecular Crystals, Springer US2012.
[3] T.H. Ning, Electron trapping in SiO2 due to electron-beam deposition of aluminum, Journal of Applied Physics, 49 (1978) 4077-4082.
[4] M. Nel, F.D. Auret, Deep-level transient spectroscopy detection of defects created in epitaxial GaAs after electron-beam metallization, Journal of Applied Physics, 64 (1988) 2422-2425.
[5] C. Christensen, J.W. Petersen, A.N. Larsen, Point defect injection into silicon due to low-temperature surface modifications, Applied Physics Letters, 61 (1992) 1426-1428.
[6] S.M.M. Coelho, F.D. Auret, P.J. Janse van Rensburg, J.M. Nel, Electrical characterization of defects introduced in n-Ge during electron beam deposition or exposure, Journal of Applied Physics, 114 (2013) 173708.
[7] M.S. Dresselhaus, R. Kalish, Ion Implantation in Diamond, Graphite and Related Materials, Springer Berlin Heidelberg2013.
[8] J.F. Archilla, N. Jiménez, V.J. Sánchez-Morcillo, L.M. Garcia-Raffi, Quodons in Mica: Nonlinear localized travelling excitations in crystals, Springer2015.
[9] H.T. Danga, F.D. Auret, S.M.M. Coelho, M. Diale, Electrical Characterisation of electron beam exposure induced Defects in silicon, Physica B: Condensed Matter.
[10] E. Omotoso, W.E. Meyer, F.D. Auret, S.M. Martins Coelho, M. Ngoepe, P. Ngako, Electrical characterization of defects introduced in n-type N-doped 4HSiC during electron beam exposure, Solid State Phenomena, 242 (2016).
[11] S.M. Sze, Semiconductor devices: physics and technology, John Wiley & Sons2008.
[12] A.R. Peaker, V.P. Markevich, I.D. Hawkins, B. Hamilton, K. Bonde Nielsen, K. Gościński, Laplace deep level transient spectroscopy: Embodiment and evolution, Physica B: Condensed Matter, 407 (2012) 3026-3030.
[13] S.M. Tunhuma, F.D. Auret, M.J. Legodi, M. Diale, The effect of high temperatures on the electrical characteristics of Au/n-GaAs Schottky diodes, Physica B: Condensed Matter, 480 (2016) 201-205.
[14] J.H. Werner, H.H. Güttler, Barrier inhomogeneities at Schottky contacts, Journal of Applied Physics, 69 (1991) 1522-1533.
[15] F. Léonard, J. Tersoff, Role of Fermi-Level Pinning in Nanotube Schottky Diodes, Physical Review Letters, 84 (2000) 4693-4696.
[16] G. Myburg, F.D. Auret, Influence of the electron beam evaporation rate of Pt and the semiconductor carrier density on the characteristics of Pt/n-GaAs Schottky contacts, Journal of Applied Physics, 71 (1992) 6172-6176.
[17] E. Omotoso, W.E. Meyer, S.M.M. Coelho, M. Diale, P.N.M. Ngoepe, F.D. Auret, Electrical characterization of defects introduced during electron beam deposition of W Schottky contacts on n-type 4H-SiC, Materials Science in Semiconductor Processing, 51 (2016) 20-24.
[18] F.D. Auret, W.E. Meyer, S. Coelho, M. Hayes, J.M. Nel, Electrical characterization of defects introduced during electron beam deposition of Schottky contacts on n-type Ge, Materials Science in Semiconductor Processing, 9 (2006) 576-579.
[19] F.D. Auret, P.J. Janse van Rensburg, W.E. Meyer, S.M.M. Coelho, V. Kolkovsky, J.R. Botha, C. Nyamhere, A. Venter, Inductively coupled plasma induced deep levels in epitaxial n-GaAs, Physica B: Condensed Matter, 407 (2012) 1497-1500.
[20] J.A. Naber, Semiconductors and Semimetals, Elsevier Science2014.
[21] L. Bischoff, R. Böttger, K.H. Heinig, S. Facsko, W. Pilz, Surface patterning of GaAs under irradiation with very heavy polyatomic Au ions, Applied Surface Science, 310 (2014) 154-157.
[22] I.K. Danileiko, T. Lebedeva, A. Manenkov, A. Sidorin, Investigation of mechanisms of damage to semiconductors by high-power infrared laser radiation, Zhurnal Eksperimentalnoi i Teoreticheskoi Fiziki, 74 (1978) 765-771.

Table I: Diode parameters of low doped *n*-GaAs Schottky diodes exposed to an electron beam (EBE), fabricated by electron beam physical vapour deposition (EB-PVD), fabricated by resistive evaporation (RE) and exposed to high energy electron irradiation (HEEI).

Process	n	ϕ_{IV} (eV)	ϕ_{CV} (eV)	Current at -1V (A)	Contact metal
EBE	1.17	0.84	1.02	7.10×10^{-7}	Au
EB-PVD	1.29	0.78	0.91	1.63×10^{-7}	W
RE	1.03	0.86	1.02	2.76×10^{-10}	Au
HEEI	1.09	0.84	0.98	1.50×10^{-9}	Au

Table II : Summary of electronic properties of defects induced in *n*-GaAs by electron beam exposure (EBE), electron beam physical vapour deposition (EB-PVD) and high energy electron irradiation (HEEI).

Process	Defect label	$E_T \pm 0.01$ (meV)	$\sigma_n \pm 1\%$ (cm^{-2})
EBE	$E_{0.34}$	34.6	8.2×10^{-16}
EB-PVD	$E_{0.43}$	43.3	6.5×10^{-15}
HEEI	$E_{0.14}$	13.5	3.0×10^{-15}
	$E_{0.17}$	17.1	3.4×10^{-13}
	$E_{0.38}$	38.2	7.4×10^{-16}
	$E_{0.63}$	63.4	1.0×10^{-15}

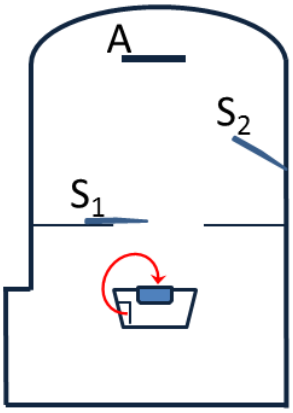

Figure 1: Schematic representation of electron beam evaporator. The arrow shows a typical path followed by an electron beam towards the metal target. S_1 and S_2 are shields for stray electrons. A is the semiconductor sample

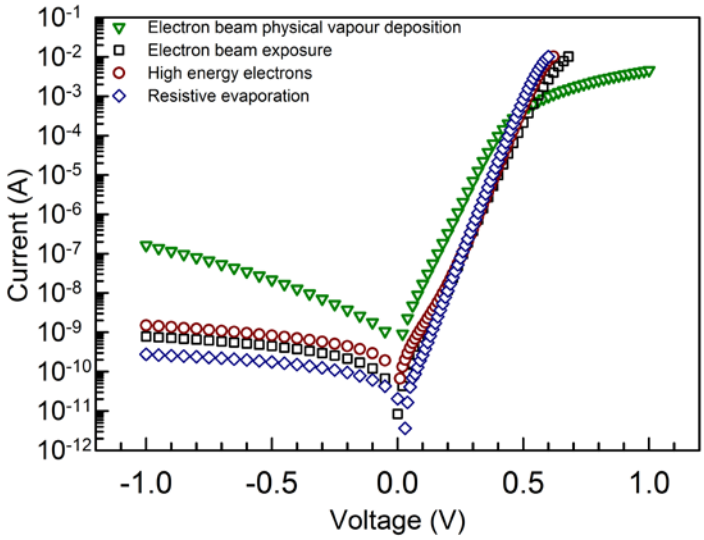

Figure 2: I-V characteristics of Schottky barrier diodes on low doped n-GaAs exposed to an electron beam (EBE), fabricated by electron beam physical vapour deposition (EB-PVD), and fabricated by resistive evaporation (RE) and exposed to high energy electron irradiation. (HEEI)

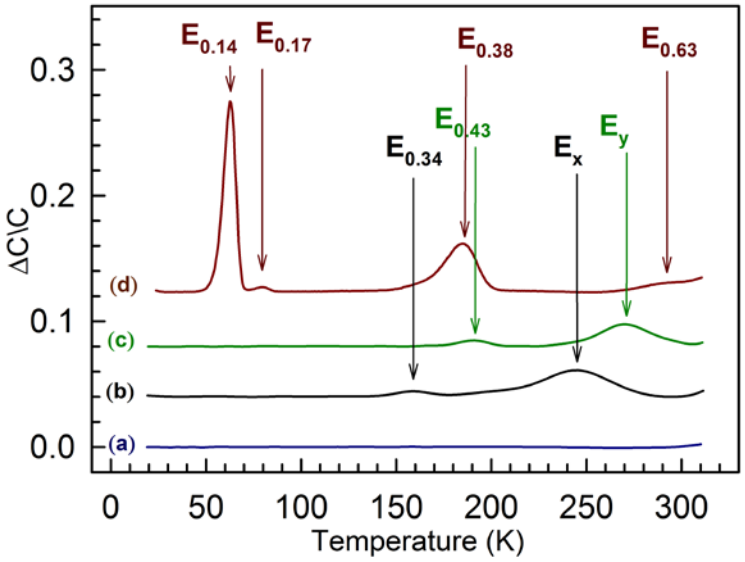

Figure 3: DLTS spectra of (a)The reference spectrum obtained from RE deposited Au/n-GaAs SBDs (b) EB-PVD fabricated W/n-GaAs SBDs (c) EBE Au/n-GaAs SBDs (d) Au/n-GaAs Schottky diodes exposed to HEEI, recorded at a quiescent reverse bias of -2.0 V, rate window of 4 Hz, and a filling pulse of 0.2V with a width of 1ms. (The E_x and E_y signatures where speculated to be a continuum of defect states).

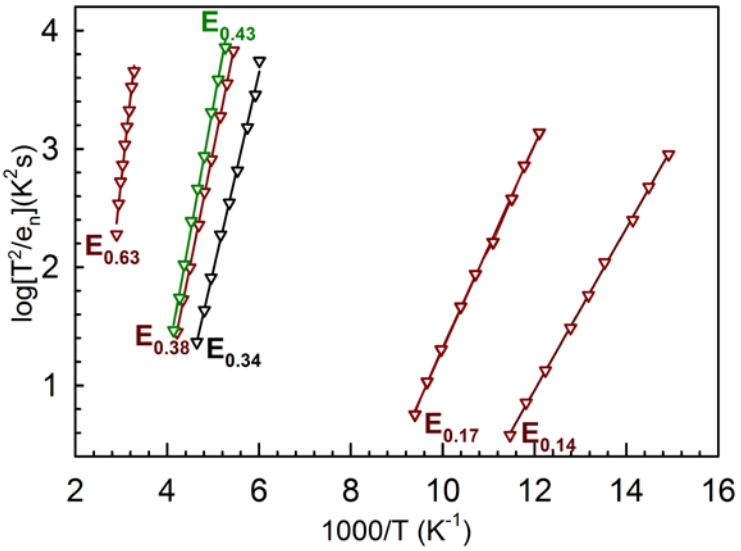

Figure 4: Arrhenius plots for defects introduced by (EBE), electron beam physical vapour deposition (EB-PVD) of tungsten and high energy electron irradiation (HEEI).